Enhanced Electron Transport and Heat Transfer Boost Light Stability of Ternary Organic Photovoltaic Cells Incorporating Non-Fullerene Small Molecule and Polymer Acceptors

Hang Yin, Ka Lok Chiu, Pengqing Bi, Gang Li, Cenqi Yan, Hua Tang, Chujun Zhang, Yiqun Xiao, Hengkai Zhang, Wei Yu, Hanlin Hu, Xinhui Lu, Xiaotao Hao, Shu Kong So

H. Y. and K. L. C. contribute equally in this work.

Dr. H. Yin, C. Yan, Prof. G. Li

Department of Electronic and Information Engineering

The Hong Kong Polytechnic University

Hung Hom, Kowloon, Hong Kong SAR, China

Email: gang.w.li@polyu.edu.hk

K. L. Chiu, C. Zhang, Prof. S. K. So

Department of Physics and Institute of Advanced Materials

Hong Kong Baptist University

Kowloon Tong, Hong Kong SAR, P.R. China

E-mail: skso@hkbu.edu.hk

Abstract

Operation stability remains the key hurdle for the best-performed non-fullerene (NF) small molecule acceptor (SMA) based organic photovoltaic (OPV) devices. Among all SMAs, ITIC-derivative is the leading contender for power conversion efficiencies >14%. However, the operation stability of the SMA-based devices under illumination is relatively inferior when compared to BHJ cells that employ or polymeric acceptors. Here, we use a polymer acceptor N2200 as the third component to study the device performance of the ITIC-derivative-based PBDB-T:ITIC-M and PBDB-T-2F:IT-4F bulk-heterojunction (BHJ) solar cells, which current are the state-of-the-art high performance OPV devices. The N2200-based ternary solar cells enjoy significantly improved operation stability, while maintaining high power conversion efficiency (PCE). We conducted comprehensive mechanism study on the ternary OPV systems in (i) electronic and (ii) thermal aspects. For (i), the ternary BHJs show remarkably improved electron transport properties. For (ii), thermal diffusivity *D*, is introduced into the OPV field for the first time, and successfully correlates with the operation stability. The ternary PBDB-T:N2200:ITIC-M BHJ exhibits improved *D* values, indicating heat generated from incident photons dissociates easily in such films.

Article

Solution-processed organic photovoltaic (OPV) devices have attracted considerable attention for their potential in fabricating flexible, low-cost, low thermal budget, and lightweight solar panels.[1-4] Over the past decades, great efforts have been devoted for high performance organic solar cells (OSCs). These efforts include development of new material synthesis, fine tuning the donor:acceptor (D:A) compositions, and the optimization of fabrication process.[5-12] A key accomplishment of these efforts is the identification of small molecule acceptors (SMAs). In

particular, BHJs using SMAs of ITIC-based acceptors can attain both high V_{oc} and J_{sc}. With fused-ring electron acceptors (FREAs), the highest record power conversion efficiencies (PCEs) for the single junction bulk heterojunction (BHJ) and tandem OPV devices have gone beyond 15% and 17%, respectively.[13,14] (Joule…)

Besides the efficiency, the processibility and stability are also important for industrial applications.[15,16] However, at present, there is a general lack in understanding the operation stability of the high efficiency SMA-based devices. To address this knowledge gap, here we first report mechanism investigations on the bench-marked binary BHJs of PBDB-T:ITIC-M and PBDB-T-2F:IT-4F. The BHJ uses SMA IT-4F as the acceptor and high PCEs exceeding 12% has been reported. However, we found the photostability of their BHJs is far from satisfactory. **Figure 1** shows the operation stability of the PBDB-T:ITIC-M and PBDB-T-2F:IT-4F BHJ cells. An initial PCE of 12.3% was achieved in PBDB-T-2F:IT-4F device, but the PCE decays steadily under continuous simulated 1-Sun illumination condition (using white LED). After about 170 hours, the PCE drops to only about 5%. As a comparison, we replace ITIC-derivatives with a polymer acceptor N2200 in the BHJ to form an all-polymer solar cell. Although the initial PCE of the all-polymer device is only ~6% (half of the PBDB-T-2F:IT-4F case), the N2200-based device exhibits much improved device stability. After 150 hours under illumination, the all polymer device's PCE (~5.5%) surpasses that of the PBDB-T-2F:IT-4F device. (Scale 0-13…)

Here, aiming at addressing the stability problem, we conducted thorough mechanism investigation of ternary OPV by incorporating (full name) N2200 as the third component. Ternary OPV devices are known to enhance the efficiency, processibility, and stability in selected parent binary OPV cells.[17-20] For example, Li, Yang and co-workers elucidate the importance of polymer donors' molecular structure compatibility on BHJ morphology in ternary OPVs with multiple polymer

donors (PCBM as acceptor).[21] Lu et al. and Bi et al reported the Förster resonance energy transfer effects in ternary OPV devices, respectively.[22,23] Liu et al. fabricated a polymer:bi-acceptor PM6:ITCPTC:MeIC ternary solar cell achieving an overall PCE of 14.13%, with a high FF of 78.2%, compared to 13.04% and 12.31% of their counterpart binary devices. [24] Zhang et al. selected a small molecule donor BTR blending into the PTB7-Th:$PC_{71}BM$ BHJs, and a thick-film (250nm) device exhibits a high PCE of 11.40%.[25] Recently, An et al. observed the ternary PBDB-T:ITIC:N2200 BHJ solar cells, which enjoys enhanced device stability in the ambient air, and over 80% of the normalized PCE is reserved in such a ternary device after 1000 hour.[26] Add PKU ternary papers…

In this report, we use a polymer acceptor N2200 as a ternary component to address the problem of the relatively low operation stability of FREA-based BHJ solar cells. Two binary BHJ systems invested are PBDB-T:ITIC-M and PBDB-T-2F:IT-4F solar cells. The improvement of the N2200-added ternary BHJ solar cells are mainly in two aspects: (i) improved FF and PCE of the ternary OPV cells with only a tiny dosage (2.5 wt%) of N2200; and (ii) a 10 wt% N2200 loading significantly stabilizes the ternary devices under the simulated 1-Sun illumination condition. The PBDB-T:ITIC-M BHJ is selected as the model system to investigate the mechanism of the stability improvement. We investigate both the charge transport and heat diffusion in the ternary BHJs. Our results indicate that the ternary BHJs with N2200 show significantly improved electron mobilities starting at a very low N2200 dosage and reduced electron energetic disorder σ_e than binary PBDB-T:ITIC-M film. Photothermal deflection technique was used to measure heat diffusivities (*D*) in the binary and ternary films, and the ternary PBDB-T:N2200:ITIC-M BHJ exhibits much improved *D* values.

Figure 2 summarizes the chemical structures of the donor polymers (PBDB-T, PBDB-T-2F, and PBDB-T-2F), SMAs (ITIC-M, and IT-4F), and the polymer-acceptor N2200. The device structure is ITO/PEDOT:PSS/BHJ/PFN-Br/Ag. **Figure 3(a)** shows the current density – voltage (J-V) characteristics of the binary PBDB-T:ITIC-M, PBDB-T:N2200 and the ternary PBDB-T:N2200:ITIC-M (weight ratios of 100:2.5:97.5/100:10:90) solar cells. The PBDB-T:ITIC-M device shows an overall PCE of 10.2%, with J_{sc} of 17.2 mA/cm^2, FF of 65.1%, and V_{oc} of 0.91V. With 2.5 wt% N2200, the ternary devices exhibit enhanced PCE of 10.7%, which shows increased FF of 70.4%. The excessive N2200 in the blending film decreases the FF and J_{sc} in the ternary cells, and the PCE of the ternary solar cell with 10 wt% N2200 decreases to 9.3%. Figure 3(b) displays the external quantum efficiency (EQE) spectra of the optimized binary PBDB-T:ITIC-M, PBDB-T:N2200, and the ternary PBDB-T:N2200:ITIC-M (10 wt% N2200) solar cells. Figure 3(c-e) plots the OPV parameters of the PBDB-T-based solar cells as a function of the N2200 weight content. After the peak PCE 10.7% at 2.5 wt%, the PCE drops and the PBDB-T:N2200 device shows PCE of 6.4%, with J_{sc} of 12.8 mA/cm^2, FF of 62.2%, and V_{oc} of 0.80 V.

Space-charge-limited current (SCLC) was performed to test the electron mobilities of BHJs with different N2200 weight contents. The device structure of the electron-only device is ITO/Al/BHJ/LiF/Al. For a given BHJ, the SCLC mobilities of BHJs can be expressed as

$$J_{SCL}d = \frac{9}{8}\varepsilon_0\varepsilon_r\mu_0 \exp(0.89\beta\sqrt{F})F^2 \quad (1)$$

where J_{SCL} is the density of the space-charged-limited current, d is the thickness of the BHJ film, ε_0 is the permittivity of a vacuum, ε_r is the relative permittivity, μ_0 is the zero-field mobility, β is the Poole-Frenkel slope, and F is the applied electric field. [27-29] After the device fabrication, the electron-only cells were transferred into a low vacuum cryostat (~30 mbar) to measure the

electron transport signal. **Figure 4(a)** displays the electron current density (J) × film thickness (d) of the PBDB-T:N2200:ITIC-M BHJs with different N2200 contents as a function of the applied electric field. The BHJs with N2200 exhibit larger $J \times d$ values than the PBDB-T:ITIC-M film, especially in the low electric field condition, where the OPV cells usually operate. Fitted by Eq. 1, the zero-field electron mobility of the control binary PBDB-T:ITIC-M BHJ is 4.7×10^{-7} $cm^2V^{-1}s^{-1}$. The $\mu_{0,e}$ improves significantly to 3.4×10^{-5} $cm^2V^{-1}s^{-1}$ when 10 wt% N2200 is blended into the BHJ film, and maintains in the range of 10^{-5} - 10^{-4} $cm^2V^{-1}s^{-1}$ in BHJs with other N2200:ITIC-M weight ratios. Figure 4(c) shows the zero-field electron mobilities at the room temperature of BHJs shown in Figure 4(a), and **Table 1** lists the electron transport parameters in this work.

Temperature-dependent electron transport measurements were performed to evaluate the electron energetic disorders σ_e and the high temperature limited mobilities μ_∞ of PBDB-T-based BHJ films. The Gaussian disorder model (GDM) is used to analyze the temperature-dependent electron mobilities i.e.

$$\mu_0 = \mu_\infty exp\left[-\left(\frac{2\sigma}{3kT}\right)^2\right]\exp\left(\beta\sqrt{F}\right) \quad (2)$$

where k is the Boltzmann constant, and μ_∞ is the y-intercept from the plot of μ_0 against $1/T^2$.[30-33] Figure 4(b) plots $\mu_{0,e}$ of PBDB-T-based BHJs with various N2200 weight contents as a function of the temperature. With the blending of N2200, the ternary BHJs exhibit improved electron mobilities in different temperatures. σ_e can be extracted from the slope of the linear fitting for the temperature-dependent electron mobilities. Compared to σ_e of 62 meV in the binary PBDB-T:ITIC-M BHJ, the ternary BHJs with N2200 first interestingly exhibit a reduced σ_e at 10% N2200 loading – 57 meV, correlates well with the enhanced zero field mobility at this composition.

Further increasing N2200 loading leads to increased σ_e, due to the intrinsically higher σ_e of N2200 polymer (~100 meV). Figure 4(d) summarizes the σ_e of BHJ films.

From Figure 4(b), the high-temperature limited electron mobilities $\mu_{\infty,e}$ can be extracted from the y-intercept of the linear mobility fitting curve. In organic semiconductor materials, electrons overcome energetic barriers and hop freely between different hopping sites when the temperature tends to be infinitely high. Figure 4(e) compares $\mu_{\infty,e}$ of BHJ films with different N2200:ITIC-M compositions, and the $\mu_{\infty,e}$ values increase gradually when more N2200 acceptor is blended into the BHJs. $\mu_{\infty,e}$ can be expressed as

$$\mu_{\infty,e} = \frac{e\nu_0\alpha^2}{\sigma_e}\exp\left(\frac{-2\alpha}{L}\right) \quad (3)$$

where α is the average hopping distance, ν_0 is the attempt-to-hop frequency, e is the elementary charge, and L is the localized radius.[34] The hopping distance can be extracted from the crossing point between the $\mu_{\infty,e}$ expressed in Eq. 3 and the values from Figure 4(b). Figure 4(f) shows the average hopping distance of the electron carriers in PBDB-T-based BHJs with different N2200 weight fractions. It is clear to observe that with the increased N2200 molecules, α decreases consistently from 3.5 nm in pure PBDB-T:IT-M cell, to 0.83 nm in the binary all polymer PBDB-T:N2200 BHJ device. As a fraction of electron carriers transport in long-chain polymer acceptors in PBDB-T:N2200:ITIC-M BHJs, they exhibit reduced hopping distance (α), and therefore, significantly improved zero-field electron mobilities $(\mu_{0,e})$.

The optical stability under illumination is evaluated for the binary PBDB-T:ITIC-M and ternary PBDB-T:N2200:ITIC-M (weight fraction of 100:10:90) BHJ solar cells. The BHJ solar cells are encapsulated in the N_2 filled glove box, then transferred into the ambient air, and exposed under

an LED array, where the optical intensity is set equivalent to 1-Sun condition of 100 mW/cm^2. As shown in **Figure 5(a,b)**, although the initial efficiency of the ternary device is reduced to 9.3% comparing to the 10.2% of the control binary cell due to the loss of the J_{sc}, the ternary device enjoys much enhanced optical stability. After illumination for 120 hours, the binary PBDB-T:ITIC-M cell already degraded to an overall PCE of 5.8%, with significantly reduced FF of 45.5%, whereas the ternary device with 10 wt% N2200 still maintains an efficiency of 7.8%, which reserves ~84% of its initial device performance. **Figure S1(a-c)** compares the OPV parameters of the PBDB-T:ITIC-M and PBDB-T:N2200:ITIC-M (100:10:90) devices as a function of the elapsed time under illumination. For the decay behavior of the PBDB-T:ITIC-M solar cell, three main characteristics are observed: (i) the performance (PCE) decay of the binary solar cell mainly occurs in the first 72 hours; (ii) the FF is the major cause of the PCE decrease – only ~60% of the normalized FF is reserved when the device is illuminated for 240 hours; and (iii) V_{oc} is relatively stable in the illumination condition.

We also fabricate the PBDB-T-2F:N2200:IT-4F ternary BHJ solar cells. With a 2.5 wt% N2200 blending, the FF of the ternary solar cell improves to 73.9% from 70.3% of the counterpart binary device, resulting in an enhanced PCE of 12.5%. The ternary PBDB-T:N2200:IT-4F (weight ratio of 100:10:90) solar cell is selected to evaluate the optical stability in the ambient air. Figure 5(c,d) summarizes the J-V characteristics of the binary and ternary devices in fresh and after a 72-hour 1-Sun illumination. Similar with the PBDB-T-based system, the ternary PBDB-T-2F solar cells with 10 wt% N2200 enjoys much better optical stability, and still show high initial PCE of 11.9% (FF of 73.8%). After a 72-hour 1-Sun illumination, the PCE of the binary cell decays quickly to 7.5%, whereas the ternary cell still maintains PCE of 10.2% - reserving ~86% of its initial PCE values. Figure S1(d-f) summarizes the OPV parameters of the binary PBDB-T-2F:IT-4F and

ternary (10 wt% N2200) BHJ solar cells as a function of the elapsed time under illumination. The ternary PBDB-T-2F-based device again exhibits improved optical stability than their counterpart binary solar cells.

Explanation of Stability mechanism

Discussion

Thermal diffusivity *D*, with a SI unit of m^2/s, is first introduced into the OPV field, and successfully correlates with the optical stability of BHJ solar cells. The definition of *D* is the ratio between the thermal conductivity (K) to the product of mass density (ρ) and specific heat capacity (c_p) expressed as

$$D = \frac{K}{\rho c_p} \tag{4}$$

D is an important concept in the heat conduction, and the value of *D* reflects the rate of heat transfer along the heat gradient in the solid materials.[35-37] For a material with higher thermal diffusivity *D*, it reaches the thermal equilibrium in a short time when the heat gradient exists. Electrons in BHJs absorb incident photons and jump into the excited states when the OPV device is in operation under the 1-Sun illumination. The recombination process which electrons drop back to the ground state and releases photons has the adverse effects in two aspects: (i) FFs/Jscs; and (ii) device stability.[38,39] For (i), how the carrier recombination affects the device performance has been well investigated and modeled elsewhere.[40-42] However, there are relatively few studies about

the correlation between photons generated from the electron and device stability is relatively. Here, we evaluate the thermal diffusivity *D* in the neat acceptor films and their corresponding binary and ternary BHJs. **Figure 6(a)** shows the photothermal deflection signal against the pump beam offset of ITIC-M film with different modulating frequency (*f*). When *f* increases, both the central peak of the normal deflection signal and separation between two minimums (d_n) decrease. Figure 5(b) displays the relation of d_n and $1/\sqrt{f}$, and the slope of this plot equals to $\sqrt{\pi D}$. As shown in Figure 5, the *D* value of the neat ITIC-M is 0.65 ± 0.09 mm^2/s, which is lower than 1.00 ± 0.13 mm^2/s of the N2200 film, indicating a better heat dissociation in the polymer acceptor N2200. In the D:A blending films, the binary all-polymer PBDB-T:N2200 BHJ exhibits a highest *D* value of 2.00 ± 0.16 mm^2/s, and this result is consistent with the excellent device stability in literatures.[43-45] When the binary PBDB-T:ITIC-M BHJ with a poor *D* value of 0.062 ± 0.060 mm^2/s is blended with 10 wt% N2200, its thermal diffusivity *D* boosts up to 0.56 ± 0.08 mm^2/s, indicating significantly enhanced heat dissociation. As shown in Figure 4, the optical stability is improved in such a ternary BHJ solar cell.

In this report, a polymer acceptor N2200 is introduced as a ternary component to address the problem of the relatively low operation stability of ITIC-based BHJ solar cells involving PBDB-T:ITIC-M and PBDB-T-2F:IT-4F devices. Both the charge transport and heat diffusion in the binary and ternary BHJs are investigated, and the results suggest that the ternary BHJs with N2200 show significantly improved electron mobilities starting at a very low N2200 dosage and reduced electron energetic disorder σ_e than binary PBDB-T:ITIC-M film. Meanwhile, photothermal deflection technique was used to measure heat diffusivities (*D*) in the binary and ternary films, and the ternary PBDB-T:N2200:ITIC-M BHJ exhibits much improved *D* values.

References

[1] G. Li, R. Zhu, Y. Yang, Polymer Solar Cells. *Nat. Photonocs*. **2012**, *6*, 153-161.

[2] S. Günes, H. Neugebauer, N. S. Sariciftci, Conjugated Polymer-Based Organic Solar Cells. *Chem. Rev*. **2007**, *107*, 1324-1338.

[3] M. C. Scharber, D. Mühlbacher, M. Koppe, P. Denk, C. Waldauf, A. J. Heeger, C. J. Brabec, Design Rules for Donors in Bulk-Heterojunction Solar Cells – Towards 10% Energy Conversion Efficiency. *Adv. Mater*. **2006**, *18*, 789-794.

[4] C. Yan, S. Barlow, Z. Wang, H. Yan, A. K. Y. Jen, S. R. Marder, X. Zhan, Non-Fullerene Acceptors for Organic Solar Cells. *Nat. Rev. Mater*. **2018**, *3*, 18003.

[5] G. Li, W. Chang, Y. Yang, Low-Bandgap Conjugated Polymers Enabling Solution-Processable Tandem Solar Cells. *Nat. Rev. Mater*. **2017**, *2*, 17043.

[6] P. Cheng, G. Li, X. Zhan, Y. Yang, Next-Generation Organic Photovoltaics Based on Non-Fullerene Acceptors. *Nat. Photonics*. **2018**, *12*, 131-142.

[7] J. Liu, S. Chen, D. Qian, B. Gautam, G. Yang, J. Zhao, J. Bergqvist, F. Zhang, W. Ma, H. Ade, O. Inganäs, K. Gundogdu, F. Gao, H. Yan, Fast Charge Separation in a Non-Fullerene Organic Solar Cell with a Small Driving Force. *Nat. Energy*. **2016**, *1*, 16089.

[8] J. Hou, O. Inganäs, R. H. Friend, F. Gao, Organic Solar Cells Based on Non-Fullerene Acceptors. *Nat. Mater*. **2018**, *17*, 119-128.

[9] N. A. Ran, J. A. Love, M. C. Heiber, X. Jiao, M. P. Hughes, A. Karki, M. Wang, V. V. Brus, H. Wang, D. Neher, H. Ade, G. C. Bazan, T. Q. Nguyen, Charge Generation and Recombination in An Organic Solar Cells with Low Energetic Offsets. Adv. Energy Mater. 2018, 8, 1701703.

[10] W. Zhao, S. Li, H. Yao, S. Zhang, Y. Zhang, B. Yang, J. Hou, Molecular Optimization Enables Over 13% Efficiency in Organic Solar Cells. *J. Am. Chem. Soc*. **2017**, *139*, 7148-7151.

[11] C. H. Y. Ho, H. Cao, Y. Lu, T. Lau, S. H. Cheung, H. Li, H. Yin, K. L. Chiu, L. Ma, Y. Cheng, S. Tsang, X. Lu, S. K. So, B. S. Ong, Boosting The Photovoltaic Thermal Stability of Fullerene Bulk Heterojunction Solar Cells Through Charge Transfer Interactions. *J. Mater. Chem. A.***2017**, *5*, 23662-23670.

[12] G. Dennler, M. C. Scharber, C. J. Brabec, Polymer-Fullerene Bulk-Heterojunction Solar Cells. *Adv. Mater*. **2009**, **21**, 1323-1338.

[13] Z. Zheng, Q. Hu, S. Zhang, D. Zhang, J. Wang, S. Xie, R. Wang, Y. Qin, W. Li, L. Hong, N. Liang, F. Liu, Y. Zhang, Z. Wei, Z. Tang, T. P. Russell, J. Hou, H. Zhou, A Highly Efficient Non-Fullerene Organic Solar Cell with A Fill Factor over 0.80 Enabled by A Fine-Tunned Hole-Transporting Layer. *Adv. Mater*. **2018**, *30*, 1801801.

[14] L. Meng, Y. Zhang, X. Wan, C. Li, X. Zhang, Y. Wang, X. Ke, Z. Xiao, L. Ding, R. Xia, H. Yip, Y. Cao, Y. Chen, Organic and Solution-Processed Tandem Solar Cells with 17.3% Efficiency. *Science*. **2018**, DOI:10.1126/science.aat2612.

[15] K. Zhang, Z. Chen, A. Armin, S. Dong, R. Xia, H. Yip, S. Shoaee, F. Huang, Y. Cao, Efficient Large Area Organic Solar Cells Processed by Blade-Coating with Single-Component Green Solvent. *Sol. RRL*. **2018**, *2*, 1700169.

[16] H. Yin, P. Bi, S. H. Cheung, W. L. Cheng, K. L. Chiu, C. H. Y. Ho, H. W. Li, S. W. Tsang, X. Hao, S. K. So, Balanced Electric Field Dependent Mobilities: A Key to Access High Fill Factors in Organic Bulk Heterojunction Solar Cells. *Sol. RRL*. **2018**, *2*, 1700239.

[17] H. Yin, J. K. W. Ho, S. H. Cheung, R. J. Yan, K. L. Chiu, X. Hao, S. K. So, Designing a Ternary Photovoltaic Cell for Indoor Light Harvesting with a Power Conversion Efficiency Exceeding 20%. *J. Mater. Chem. A* **2018**, *6*, 8579-8585.

[18] L. Lu, M. A. Kelly, W. You, L. Yu, Status and Prospects for Ternary Organic Photovoltaics, *Nat. Photonics*. **2015**, *9*, 491-500.

[19] H. Fu, Z. Wang, Y. Sun, Advances in Non-Fullerene Acceptor Based Ternary Organic Solar Cells. *Sol. RRL*. **2018**, *2*, 1700158.

[20] L. Zhan, S. Li, H. Zhang, F. Gao, T. K. Lau, X. Lu, D. Sun, P. Wang, M. Shi, C. Z. Li, H. Chen, A Near-Infrared Photoactive Morphology Modifier Leads to Significant Current Improvement and Energy Loss Mitigation for Ternary Organic Solar Cells. *Adv. Sci*. **2018**, *5*, 1800755.

[21] Y. Yang, W. Chen, L. Dou, W. H. Chang, H. S. Duan, B. Bob, G. Li, Y. Yang, High-Performance Multiple-Donor Bulk Heterojunction Solar Cells. *Nat. Photonics*. **2015**, *9*, 190-198.

[22] L. Lu, T. Xu, W. Chen, E. S. Landry, L. Yu, Ternary Blend Polymer Solar Cells with Enhanced Power Conversion Efficiency. *Nat. Photonics*. **2014**, *8*, 716-722.

[23] P. Bi, F. Zheng, X. Yang, M. Niu, L. Feng, W. Qin, X. Hao, Dual Förster Rsonance Energy Transfer Effects in Non-Fullerene Ternary Organic Solar Cells with the Third Component Embedded in the Donor and Acceptor. *J. Mater. Chem. A* **2017**, *5*, 12120-12130.

[24] T. Liu, Z. Luo, Q. Fan, G. Zhang, L. Zhang, W. Gao, X. Guo, W. Ma, M. Zhang, C. Yang, Y. Li, H. Yan, Use of two structurally similar small molecular acceptors enabling ternary organic solar cells with high efficiencies and fill factors. *Energy Environ. Sci*. **2018**, *11*, 3275-3282.

[25] G. Zhang, K. Zhang, Q. Yin, X. Jiang, Z. Wang, J. Xin, W. Ma, H. Yan, F. Huang, Y. Cao, High-Performance Ternary Organic Solar Cell Enabled by a Thick Active Layer Containing a Liquid Crystalline Small Molecule Donor. *J. Am. Chem. Soc*. **2017**, *139*, 2387-2395.

[26] Q. An, F. Zhang, W. Gao, Q. Sun, M. Zhang, C. Yang, J. Zhang, High-efficiency and air stable fullerene-free ternary organic solar cells. *Nano Energy*. **2018**, *45*, 177-183.

[27] C. H. Y. Ho, S. H. Cheung, H. W. Li, K. L. Chiu, Y. Cheng, H. Yin, M. H. Chan, F. So, S. W. Tsang, S. K. So, Using Ultralow Dosages of Electron Acceptor to Reveal the Early Stage Donor–Acceptor Electronic Interactions in Bulk Heterojunction Blends. *Adv. Energy Mater*. **2017**, *7*, 1602360.

[28] H. Yin, K. L. Chiu, C. H. Y. Ho, H. K. H. Lee, H. W. Li, Y. Cheng, S. W. Tsang, S. K. So, Bulk-Heterojunction Solar Cells with Enriched Polymer Contents. *Org. Electron*. **2017**, *40*, 1-7.

[29] H. Yin, S. Chen, P. Bi, X. Xu, S. H. Cheung, X. Hao, Q. Peng, X. Zhu, S. K. So, Rationalizing Device Performance of Perylenediimide Derivatives as Acceptors for Bulk-Heterojunction Organic Solar Cells. *Org. Electron*. **2019**, *65*, 156-161.

[30] H. Yin, S. H. Cheung, J. H. L. Ngai, C. H. Y. Ho, K. L. Chiu, X. Hao, H. W. Li, Y. Cheng, S. W. Tsang, S. K. So, Thick-Film High-Performance Bulk-Heterojunction Solar Cells Retaining 90% PCEs of the Optimized Thin Film Cells. *Adv. Electron. Mater*. **2017**, *3*, 1700007.

[31] C. H. Y. Ho, Q. Dong, H. Yin, W. W. K. Leung, Q. Yang, H. K. H. Lee, S. W. Tsang, S. K. So, Impact of Solvent Additive on Carrier Transport in Polymer:Fullerene Bulk Heterojunction Photovoltaic Cells. *Adv. Mater. Interfaces*. **2015**, *2*, 1500166.

[32] H. K. H. Lee, Z. Li, I. Constantinou, F. So, S. W. Tsang, S. K. So, Batch-to-Batch Variation of Polymeric Photovoltaic Materials: its Origin and Impacts on Charge Carrier Transport and Device Performances. *Adv. Energy Mater*. **2014**, *4*, 1400768.

[33] H. Yin, S. Chen, S. H. Cheung, H. W. Li, Y. Xie, S. W. Tsang, X. Zhu, S. K. So, Porphyrin-Based Thick-Film Bulk-Heterojunction Solar Cells for Indoor Light Harvesting. *J. Mater. Chem. C*. **2018**, *6*, 9111-9118.

[34]

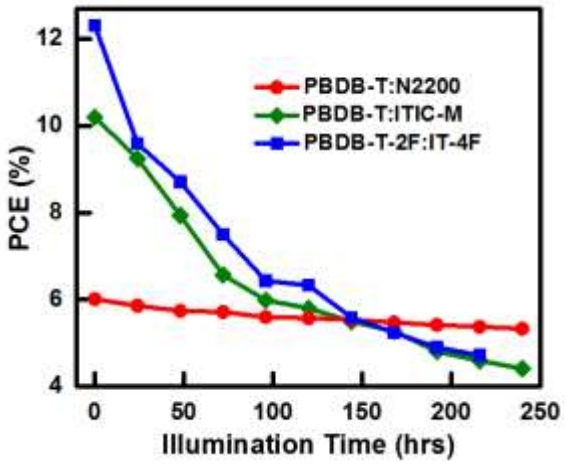

Figure 1. PCEs of the optimized SMA PBDB-T:ITIC-M and all-polymer PBDB-T:N2200 BHJ solar cells as a function of the illumination time.

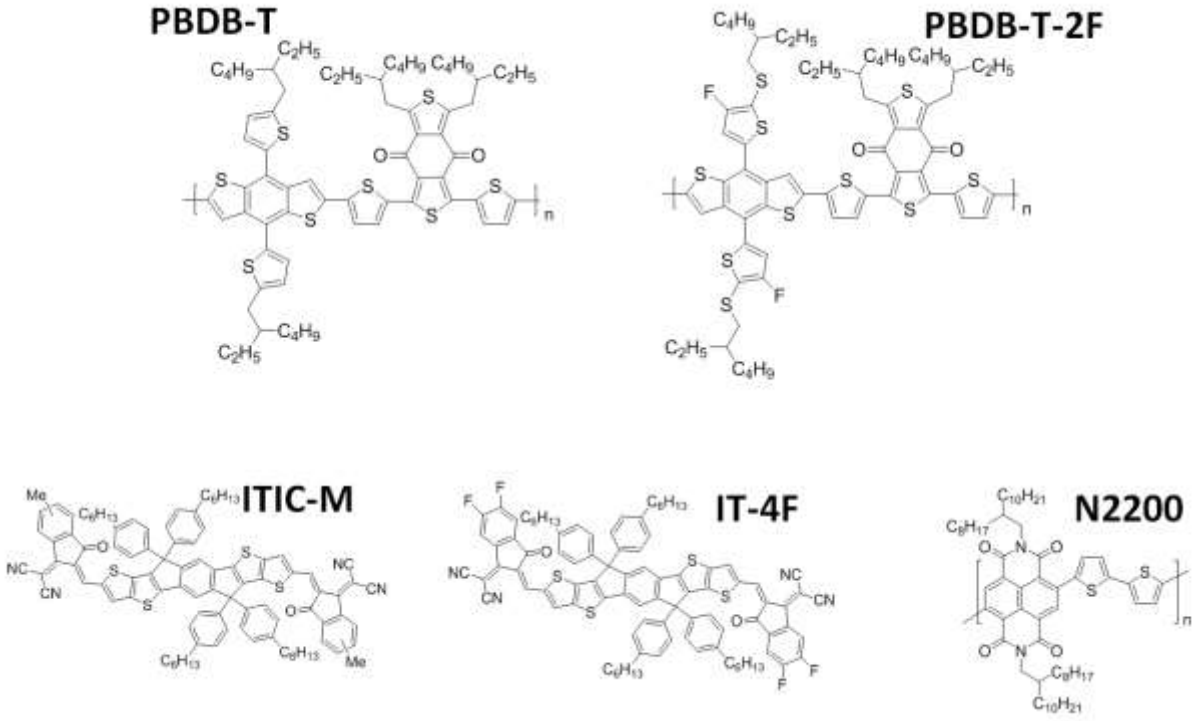

Figure 2. Chemical structures of the donor polymers PBDB-T and PBDB-T-2F, the small molecule acceptors ITIC-M and IT-4F, and the polymer acceptor N2200.

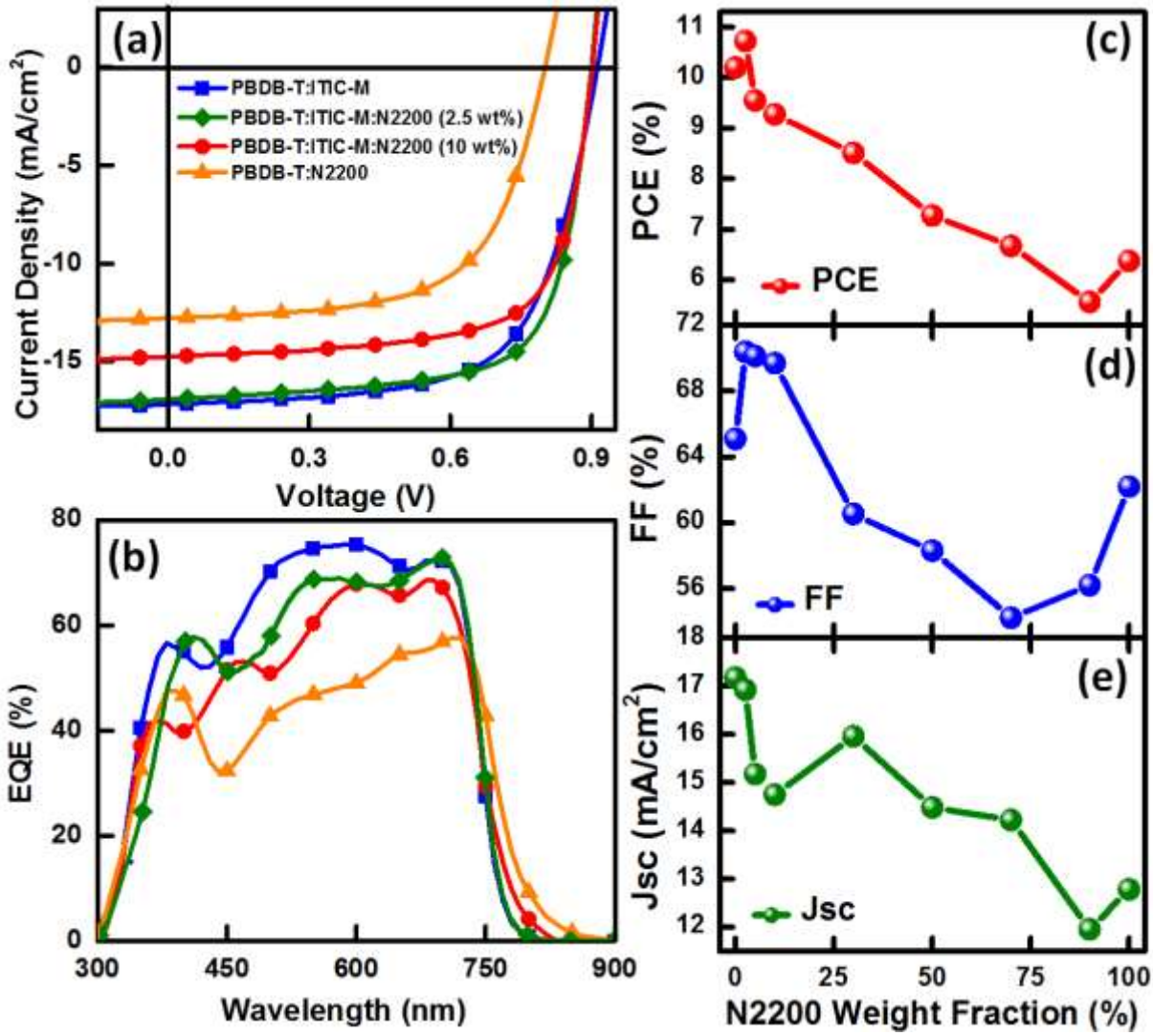

Figure 3. (a) The JV characteristics of the binary PBDB-T:ITIC-M, PBDB-T:N2200 and ternary PBDB-T:N2200:ITIC-M (weight fractions of 100:2.5:97.5/100:10:90) BHJ solar cells; (b) EQE spectra of PBDB-T:ITIC-M, PBDB-T:N2200 and PBDB-T:N2200:ITIC-M (2.5/10 wt% N2200) devices; (c) PCE; (d) FF; and (e) J_{sc} of PBDB-T:N2200:ITIC-M solar cells as a function of the N2200 weight fraction.

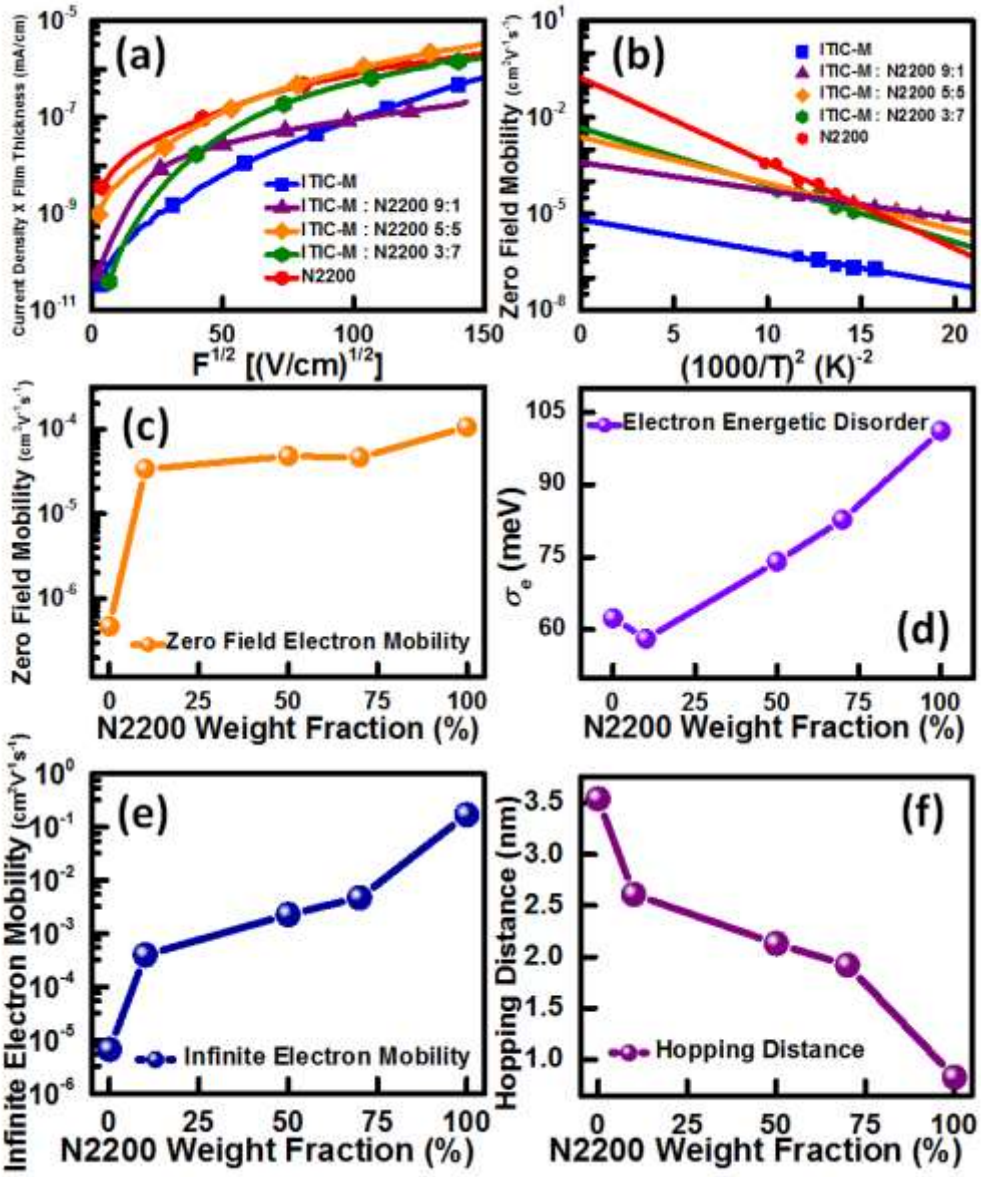

Figure 4. Electron carrier transport results for the binary PBDB-T:ITIC-M, PBDB-T:N2200, and ternary PBDB-T:N2200:ITIC-M BHJs with different N2200 weight fractions: (a) J × d as a function of the applied electric field; (b) zero-field electron mobilities in different temperatures; (c) zero-field electron mobilities at the room temperature; (d) energetic disorders of electron carriers; (e) high-temperature limited electron mobilities; and (f) hopping distances of electron carriers.

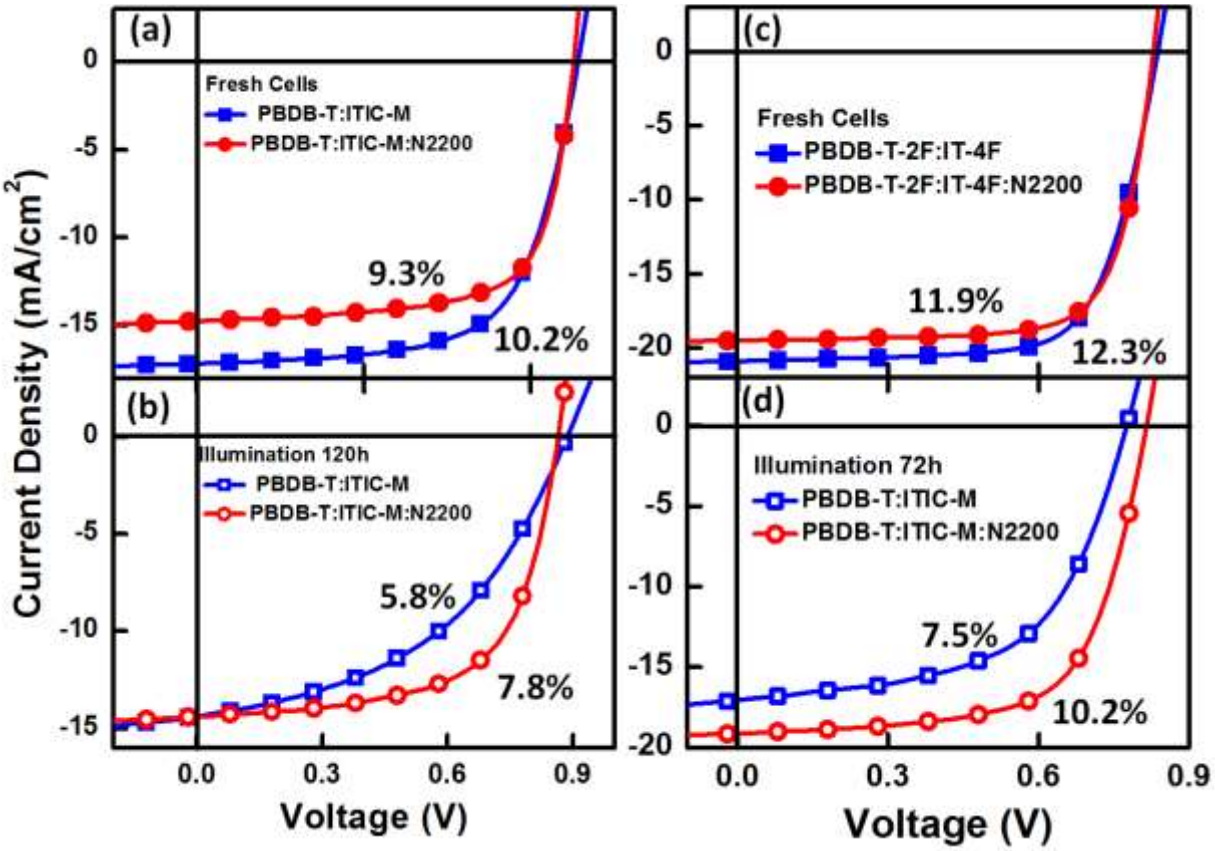

Figure 5. JV characteristics of binary PBDB-T:ITIC-M; PBDB-T-2F:IT-4F and ternary PBDB-T:N2200:ITIC-M; PBDB-T-2F:N2200:IT-4F (10 wt% N2200) BHJ solar cells before and after the 1-Sun illumination in the ambient air.

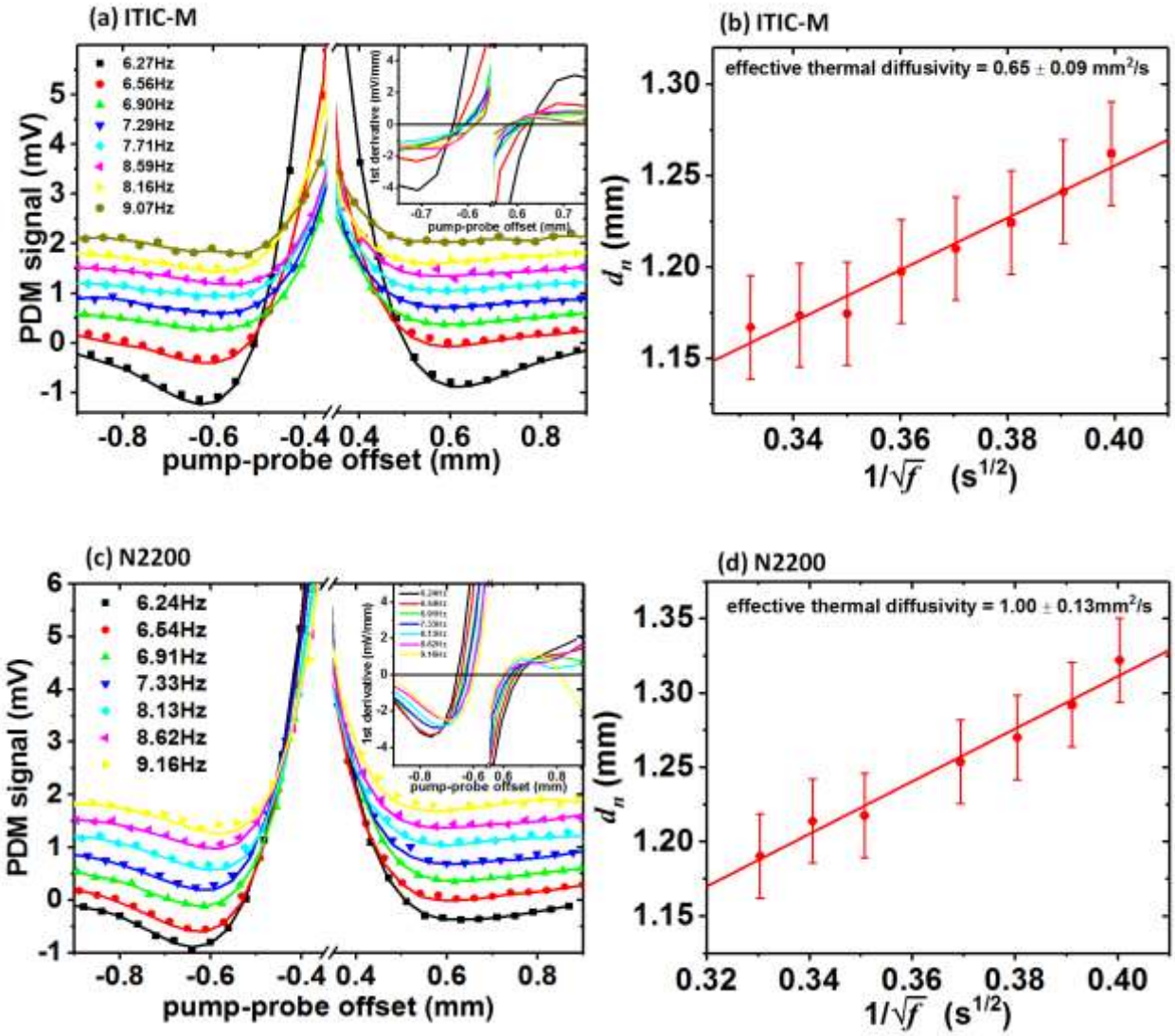
(a) ITIC-M
6.27Hz
6.56Hz
6.90Hz
7.29Hz
7.71Hz
8.59Hz
8.16Hz
9.07Hz
PDM signal (mV)
pump-probe offset (mm)
1st derivative (mV/mm)
(b) ITIC-M
effective thermal diffusivity = 0.65 ± 0.09 mm²/s
d_n (mm)
$1/\sqrt{f}$ (s$^{1/2}$)
(c) N2200
6.24Hz
6.54Hz
6.91Hz
7.33Hz
8.13Hz
8.62Hz
9.16Hz
PDM signal (mV)
pump-probe offset (mm)
(d) N2200
effective thermal diffusivity = 1.00 ± 0.13mm²/s
d_n (mm)
$1/\sqrt{f}$ (s$^{1/2}$)

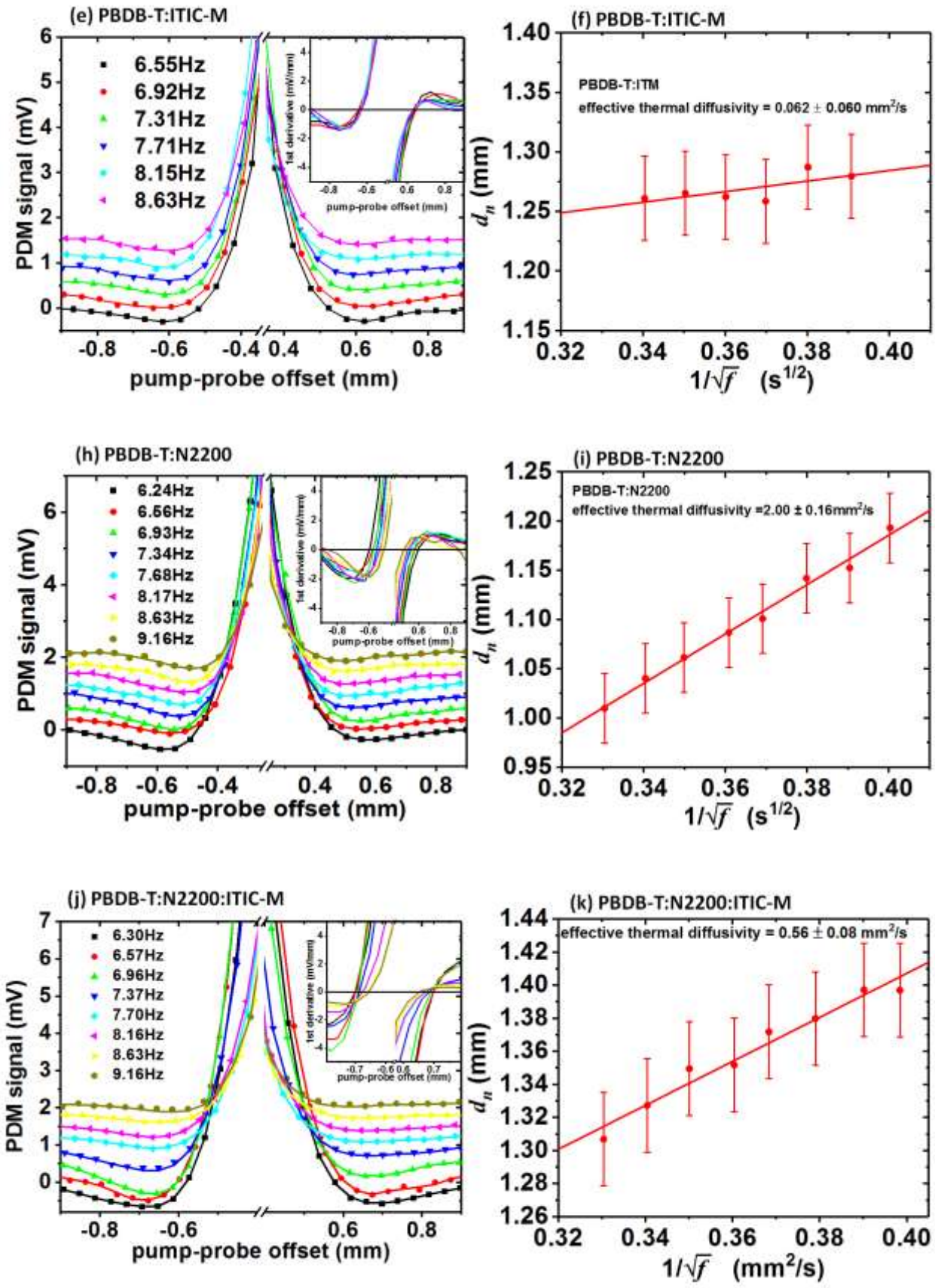
(e) PBDB-T:ITIC-M
6.55Hz
6.92Hz
7.31Hz
7.71Hz
8.15Hz
8.63Hz
PDM signal (mV)
pump-probe offset (mm)
1st derivative (mV/mm)
(f) PBDB-T:ITIC-M
PBDB-T:ITM
effective thermal diffusivity = 0.062 ± 0.060 mm²/s
d_n (mm)
$1/\sqrt{f}$ (s$^{1/2}$)
(h) PBDB-T:N2200
6.24Hz
6.56Hz
6.93Hz
7.34Hz
7.68Hz
8.17Hz
8.63Hz
9.16Hz
(i) PBDB-T:N2200
PBDB-T:N2200
effective thermal diffusivity =2.00 ± 0.16mm²/s
(j) PBDB-T:N2200:ITIC-M
6.30Hz
6.57Hz
6.96Hz
7.37Hz
7.70Hz
8.16Hz
8.63Hz
9.16Hz
(k) PBDB-T:N2200:ITIC-M
effective thermal diffusivity = 0.56 ± 0.08 mm²/s
$1/\sqrt{f}$ (mm²/s)

Figure 6. Experimental normal component of the probe beam deflection under different pump-probe beam offsets and modulating frequency; and the plot of experimental d_n against $1/\sqrt{f}$ for (a,b) neat ITIC-M film; (c,d) neat N2200 film; (e,f) binary PBDB-T:ITIC-M BHJ; (g,h) binary PBDB-T:N2200 BHJ; and (i,k) ternary PBDB-T:N2200:ITIC-M BHJ with the optimized weight fraction of 100:10:90.